Journal of Electron Spectroscopy and Related Phenomena 211 (2016) 32–40

Contents lists available at ScienceDirect

Journal of Electron Spectroscopy and Related Phenomena

journal homepage: www.elsevier.com/locate/elspec

Electron coincidence studies of sulfur-overlayers on Cu(001) and Ni(001) surfaces

G. Di Filippo[a,*,1], F.O. Schumann[a], S. Patil[a,2], Z. Wei[a], G. Stefani[b], G. Fratesi[c], M.I. Trioni[d], J. Kirschner[a]

[a] Max-Planck Institut für Mikrostrukturphysik, Weinberg 2, 06120 Halle, Germany
[b] CNISM and Dipartimento di Scienze, Università Roma Tre, Via della Vasca Navale 84, 00146 Rome, Italy
[c] Dipartimento di Fisica, Università degli Studi di Milano, Via Celoria 16, 20133 Milan, Italy
[d] CNR – National Research Council of Italy, ISTM, Via Golgi 19, 20133 Milan, Italy

ARTICLE INFO

Article history:
Received 6 April 2016
Received in revised form 20 May 2016
Accepted 2 June 2016
Available online 4 June 2016

Keywords:
Auger transition
APECS
Sulfur
Double-photoemission
Electronic structure

ABSTRACT

We have prepared different sulfur-overlayers on Cu(001) and Ni(001) surfaces which differ in their coverage and local environment of the S adatoms. Via photon absorption we excited the S 2*p* level and studied the subsequent Auger decay with a coincidence spectrometer. We discuss the variation of the coincidence rate as a function of the energy sum of the photo-Auger electron pair. This is linked to the binding energy of the double-hole state. We find that the photon energy has no dramatic influence on the spectra. Differences are observed when the local environment of sulfur is changed. The observed spectral changes are mainly ascribable to the variation of the density of states at the different surfaces. On the contrary, the strength of electron–electron correlation at the surface states is hardly affected by coverage or substrate variation.

1. Introduction

Electron emission upon photon absorption is a well-established effect used in modern spectroscopy. Besides single electron photoemission the system may also react via the emission of an electron pair [1–7]. The emitted electrons may stem from valence states or core levels. A prominent example is the Auger electron decay, following the photoemission from a core level, which is a very important tool for chemical characterization of surfaces. This process of electron pair emission upon photon absorption is termed double photoemission (DPE) and requires for its existence a non-vanishing electron–electron interaction [8]. This fact was the driving force for the development of electron pair spectroscopy from atomic, molecular and solid targets [9–19,6,20–24]. In extended systems like solids the valence states do not posses well-defined energies as in atoms, but span a range of energies due to the overlap of wave functions from neighboring sites. The properties of solids are intimately related to the details of the electronic bands and angle-resolved photoemission is an ideal probe for these states. A DPE experiment will provide information about the electron correlation within the valence band, for example the exchange-correlation hole becomes accessible in angular distributions [6,23].

Once the photon energy becomes sufficiently high to excite a core level electron above the Fermi level the system may relax via the emission of an Auger electron. If the core electron is excited into the vacuum then an electron pair is emitted. In this case we talk about core-resonant DPE. The emitted electron pairs can be detected in coincidence and this technique is usually termed Auger Photoelectron Coincidence Spectroscopy (APECS) [4,25–28].

In principle the Auger decay needs to be described in a single step [29], yet it is conventionally approximated by a two-step model. In this case the emission of the photoelectron and the Auger electron are considered as two independent processes. This model and the experimental observation of well-defined energies for the Auger and the photoelectron excludes a continuous energy sharing between the two final electrons. This prediction is at odds with studies on Cu(001) MVV [30] and Ag(001) NVV [31] Auger decay. This highlights the fact that one has to consider the pair as one entity generated in a single step event. The one step nature of the Auger process also results in the photon energy dependence of the corresponding line shape, as was observed in Xe 4*d* decay [32].

* Corresponding author.
E-mail address: gianluca.filippo@fau.de (G. Di Filippo).
[1] Current address: Lehrstuhl für Festkörperphysik, Friedrich-Alexander-Universität Erlangen-Nürnberg, Staudtstraße 7, 91058 Erlangen, Germany.
[2] Current address: Department of Physics, Indian Institute of Technology (Banaras Hindu University), Varanasi 225001, India.

http://dx.doi.org/10.1016/j.elspec.2016.06.002
0368-2048/

The Auger process proceeds such that the decay mainly takes place in the vicinity of the atom of the initial ionization. This results in an elemental sensitivity that allows to probe local electronic [33–37] and magnetic [38–41] structures. The question arises to what extent the Auger decay is modified if the local environment of the excited atom is changed.

To this end, we prepared S-overlayers on Cu(001) and Ni(001) surfaces which provided the means to vary the coverage and chemical environment. We considered the process in which the decay of a S 2*p* hole leaves the system with two vacancies in the valence band. Using coincidence spectroscopy we recorded 2D-energy distribution by reporting the number of emitted electron pairs as a function of the kinetic energies of the detected electrons. We observed a lack of energy sharing between Auger and photoelectron, which is characteristic of a sequential two-step decay. In accord with this we observed no dramatic influence of the photon energy on the spectrum line shape. Finally, we compared the measured spectra to density functional theory (DFT) calculations for the density of states on the sulfur sites. This gave us the possibility to have an insight in the changes of the electronic properties of the surfaces following the adsorption. This is an important result since the interaction of sulfur atoms with the low-index surfaces of transition and noble metals is of major interest. For example, sulfur poisoning represents one of the main issues in catalysis. The interaction with S atoms can affect both the activity and selectivity of industrial catalysts [42,43]. These effects are ascribable to the changes in the electronic structure at the very interface. It is clear that a deeper understanding of sulfur–metal interface properties is essential.

2. Experimental details

The experiments were performed with an instrument schematically depicted in Fig. 1. It consists of two hemispherical energy analyzers with the electron-optical axes of the transfer lenses perpendicular to each other [30]. More details about the set-up has been presented elsewhere [44], here we recall the key aspects. The transfer lenses define a scattering plane which lies in the *x*–*y* plane. The photon beam propagates along the *z*-axis which is perpendicular to the scattering plane and has a grazing angle of 10° with respect to the in-plane [010] direction of the sample, i.e. 80° with respect to the surface normal $\hat{n}$.

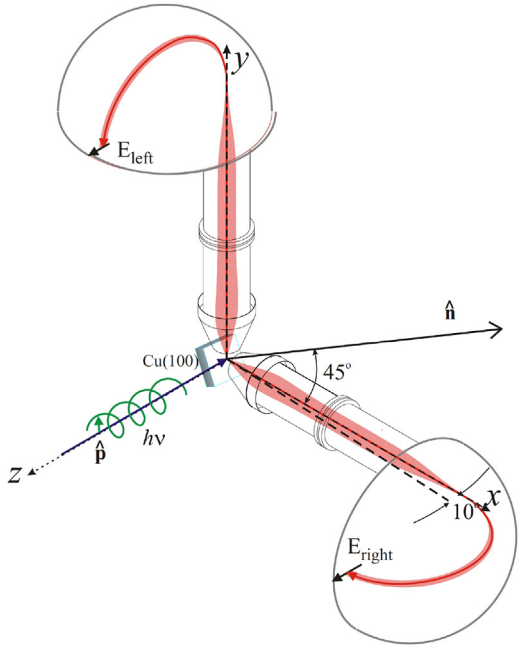

Fig. 1. The schematic view of the coincidence experiment set-up is shown. We label the two spectrometer as "left" and "right", respectively. The two transfer lenses are perpendicular to each other and define the scattering plane which lies in the *x*–*y* plane. The propagation direction of the circular polarized light is perpendicular to the scattering plane and it impinges onto the sample with an incidence angle of 80° with respect to the surface normal $\hat{n}$. The projection of the surface normal onto the scattering plane includes an angle of 45° with the two transfer lenses.

The angle between the projection of the surface normal onto the scattering plane and both transfer lenses is 45°. We operated the spectrometers with a pass energy of 300 eV and 1 mm slits. This defines a 2D-energy window of size $27 \times 27\ \mathrm{eV}^2$ in which electron pairs are detected in parallel. In contrast to the usual operation we do not scan the spectrometers' mean energy, but keep all settings fixed for a given experiment. The photon energy and the central energy of the energy window are chosen such as to allow the detection of the S 2*p* photoelectron and associated Auger electron. The energy resolution of each spectrometer was 0.8 eV. Consequently the total energy resolution for electron pairs was 1.1 eV.

We used a standard coincidence circuit which is explained in more detail elsewhere [44]. In brief, we employ a four-way coincidence circuit in which the channel plate signals originating from the two detectors have to be within a time interval of 100 ns while at the same time the electronics of the resistive anodes indicate a successful impact position determination. The knowledge of the impact position on the respective channel plate is required for the energy determination of the detected electron. The coincidence intensity has two contributions usually referred to as "true" and "random" coincidences. In the case of "true" events a single photon causes the emission of an electron pair, while "random" events are due to the absorption of two photons. Experimentally it is not possible to separate between these contributions. However one can remove the aggregate effect of the "random" coincidences by following standard procedures documented in the literature [25,26]. We described the implementation of these for our instrument previously [44]. We will present energy spectra corrected in this manner. In our studies the single count rates ranged between 3000 and 6000 cps depending on the photon energy. The total coincidence count rate was 3–7 cps with a true to random ratio of 3–4. All kinetic energies are stated with respect to the vacuum level of the sample. The experiments were performed at room temperature and the base pressure was 5×10^{-11} mbar. Circular polarized light was obtained at the beamline UE56/2-PGM-2 of the BESSY II storage ring at Helmholtz-Zentrum Berlin [45]. The preparation of the Cu(001) surface followed standard procedures consisting in Ar^+ sputtering and annealing. Besides the substrate we prepared two other surfaces, namely a Ni(001) surface and a $2\sqrt{2} \times \sqrt{2}R45°$O-Cu(001) structure. The Ni(001) surface was obtained via e-beam evaporation onto the Cu(001) surface. It is well-established that this results in a well-ordered Ni(001) surface [46–49]. Likewise, the preparation of the O-Cu(001) structure is well established in the literature [50–52]. We prepared S overlayers on these structures by H_2S dosing, for which we used a doser following a design proposed in [53]. The saturation structures obtained are in agreement with results in the literature [54,55] as we will discuss in the next section.

3. Results and discussion

There exist a vast amount of literature on the preparation of sulfur overlayers on metal surfaces and their properties in particular on Cu(001) and Ni(001) surfaces [54,55,60,56–59]. We prepared S overlayers onto the surfaces via H_2S exposure. In order to establish the conditions to give the saturation S coverages we performed ancillary studies in a separate experimental apparatus. This was equipped with a Low Energy Electron Diffraction optics and Auger

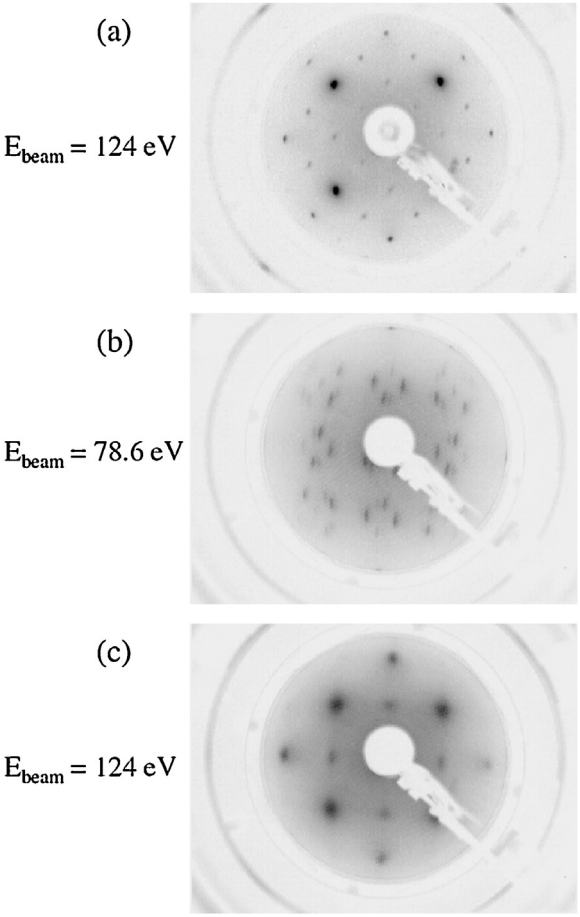

Fig. 2. LEED images obtained for (a) S/Cu(001), (b) S/O/Cu(001) and (c) S/Ni(001). The saturation coverages correspond to 0.25 ML, 0.47 ML and 0.5 ML, respectively.

spectrometer. The parameters deduced in this preparatory work were used in the coincidence study. The S/Cu(001) films were prepared by exposing the Cu(001) substrate to H_2S gas for 20 L at room temperature as laid out in the literature [54]. In order to increase the dosing efficiency, the exposure was carried out using a mechanical doser [53]. This increases the dosing efficiency by a factor ≈12. The sample was kept about 5 cm away from the doser end during the exposure. The samples were subsequently annealed at 300 °C. The saturation structure on a Cu(001) surface is of p(2 × 2) symmetry [54]. This amounts to a S coverage of 0.25 monolayers (ML). An exemplary LEED image is presented in Fig. 2(a) which agrees with the findings in the literature [54,57–59]. Exposing a Cu(001) surface to 8000 L of oxygen while the temperature is 230 °C leads to a well-known missing row reconstruction $2\sqrt{2} \times \sqrt{2}R45^\circ$ [50–52]. We will abbreviate this surface as O/Cu(001) in the following. Upon H_2S exposure following the same procedure as for the bare Cu(001) surface a $\begin{vmatrix} 5 & 2 \\ 0 & 5 \end{vmatrix}$ structure evolves. This is equivalent to a S coverage of 0.47 ML [55]. It is important to point out that the S atoms are not only on top of the surface, but also incorporated in the Cu matrix. This means that the local environment for the two adsorption sites is different. It is well-established that high quality Ni films on a Cu(001) substrate can be grown. We prepared a 10 ML thick Ni film at room temperature and exposed it to 20 L. This develops into a c(2 × 2) structure in agreement with work on bulk Ni(001) surfaces [60]. During the exposure the Ni film was kept a temperature of 150 °C. In Fig. 2 we display the LEED images for the three S surfaces investigated in this study.

Before we present the coincidence spectra we want to define some important energy relations. To be specific we assume a metallic sample. In a direct DPE experiment probing the valence band two electrons from the occupied states are emitted, which are characterized by binding energies E_{b1} and E_{b2}. We use the convention that these values are referenced to the Fermi level and are positive. The emitted electrons are detected with kinetic energies E_{left} and E_{right}. We quote the kinetic energies with respect to the vacuum level of the sample. In the energy balance we have to consider the work function ϕ of the sample. In this derivation we made the important assumption that the minimum energy required to get an electron pair into the vacuum is equal to twice the work function. This corresponds to neglecting electronic interactions in the final state. The above approximation is reasonable due to collective screening of electron–electron and hole–hole interaction. Finally, energy conservation reads as:

$$h\nu - E_{b1} - E_{b2} = E_{left} + E_{right} + 2\phi = E_{sum} + 2\phi. \quad (1)$$

Simple rearrangement leads to:

$$E_{sum} = h\nu - E_{b1} - E_{b2} - 2\phi. \quad (2)$$

In the above equations we have introduced the important quantity of the sum energy of a pair as $E_{sum} = E_{left} + E_{right}$. This emphasizes the need to regard the electron pair as one entity. The general observation from our DPE valence band studies is that a given value of E_{sum} can be attained for different combinations of E_{left} and E_{right}. The same has been identified by DPE experiments on noble gas atoms [61,62]. We label the upper bound of the sum energy as $E_{sum}^{\max}$ which is realized if both electrons originate from the Fermi level. Therefore we can write:

$$E_{sum}^{\max} = h\nu - 2\phi. \quad (3)$$

If the excitation leads to an emission of a core photoelectron and subsequent Auger decay the sum energy of this pair is given by:

$$E_{sum}^{core} = (h\nu - E_b^{core} - \phi) + E_{Auger}. \quad (4)$$

The kinetic energy of the Auger electron is labeled with E_{Auger} while the binding energy of the core level is given by E_b^{core}. In this equation the work function occurs only once, because the kinetic energy of the Auger electron is already referenced to the vacuum level of the sample. It includes relaxation and correlation terms. It is important to realize that core-resonant and direct DPE final state energies are in general different even if this involves a CVV Auger transition. This is because, contrary to direct DPE, the Auger decay is mainly localized onto the atom of the core-hole ionization. Consequently, the Auger line can be shifted to lower sum energies by a quantity that is proportional to the on-site Coulomb correlation energy U, i.e. the energy required to localize two single holes on the same atomic site [63–65].

After these definitions we proceed and display in Fig. 3 the 2D-energy spectra measured on a S/Cu(001) sample with the photon energies $h\nu$ = 301, 313 and 324 eV. These spectra were measured for two different light helicities. However, since there was no measurable dichroic effect we present helicity integrated data. The total true counts are 1.05×10^5, 2.23×10^5 and 4.45×10^4, respectively.

The 2D-energy distribution of Fig. 3(a) is described by intensity bands which are either parallel to the x- or y-axis. These intensity bands are further subdivided into two smaller regions. If we extend the vertical intensity regions to the x-axis we find intercepts at E_{right} = 133.7 and 134.8 eV, respectively. The 1.1 eV energy separation between these regions corresponds to the spin-orbit splitting of S 2p levels [66]. So we identify these as the $2p_{1/2}$ and $2p_{3/2}$ photoelectron lines, respectively. If the electron detected by the right spectrometer is a photoelectron the electron detected by the left spectrometer is an Auger electron with E_{Auger} approximately

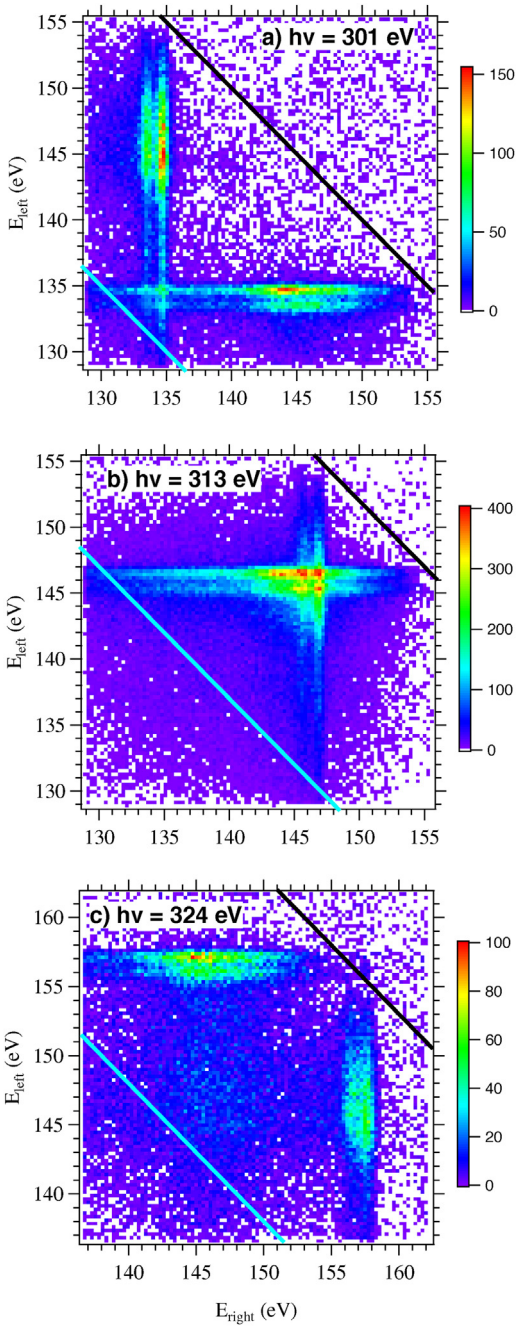

Fig. 3. 2D-energy spectra of S/Cu(001) S 2*p* photoionization and subsequent LVV Auger decay for different photon energies: (a) $h\nu = 301$ eV, (b) $h\nu = 313$ eV and (c) $h\nu = 324$ eV. The solid diagonal line marks the energy position of E_{sum}^{max} while the blue line indicates the energetic position of $E_{sum}^{max} - 25$ eV. (For interpretation of the references to color in this figure legend, the reader is referred to the web version of this article.)

145 eV. In a CVV Auger transition the participating two electrons originate from any energy position within the valence band. Hence the width of the Auger electron spectrum is roughly twice the band width. The intensity distribution of Fig. 3(a) is expected if the photo and Auger electron are sequentially emitted. In particular there is no intensity band connecting the high intensity regions centered at (134 eV, 145 eV) and (145 eV, 134 eV), thus the two-step model holds.

We have added black diagonal lines in Fig. 3 which are the position of the line E_{sum}^{max} as defined in Eq. (3). This marks the energetic position in which two valence electrons from E_F are emitted. It is obvious that no intensity is observed above this line as required by energy conservation. In addition there is no visible energy sharing between the electron pairs in the vicinity of E_{sum}^{max}. We conclude that direct DPE process from the valence states yields no detectable intensity. What we observe is a photon energy dependence of the direct DPE cross-section. It is well-known that the photoemission intensity will decrease upon increasing the photon energy [67]. A similar trend is expected to hold for DPE, too [8]. Experimentally we have observed that the DPE intensity from Cu surfaces decreases by at least an order of magnitude if $h\nu$ is changed from 35 eV to 125 eV. Therefore, it is not unexpected to see a further loss in the transition probability for $h\nu = 301$ eV.

In Fig. 3(a) we note an intensity peak for $E_{left} = E_{right} \approx 135$ eV. At first sight this appears as a coincidence of two photoelectrons. This is energetically not possible with a single photon. What is observed is a coincidence of an inelastically scattered Auger electron and a photoelectron. These events, in which the two electrons have the same kinetic energy, can be observed in two different ways. In one case the photoelectron is detected by the left spectrometer and the scattered Auger electron by the right one. In the other case, the role of the two spectrometers is exchanged, with the right electron being a photoelectron and the left one being an Auger electron. This double counting disappears when one computes the sum energy spectra, as demonstrated below.

For $h\nu = 301$ eV the most probable Auger electron energy is roughly 11 eV higher than the photoelectron energy. We studied the Auger decay also for two additional photon energies. In the one case we tuned $h\nu$ such that Auger and photoelectron have overlapping energies, while in the other case the Auger electron has 11 eV lower kinetic energy. This is achieved by choosing $h\nu = 313$ and 324 eV and the resulting 2D-energy distributions are shown in Fig. 3(b) and (c), respectively. For $h\nu = 313$ eV the kinetic energies of the Auger and photoelectron overlap at $E_{left} = E_{right} \approx 146$ eV as evidenced by the intensity peak in Fig. 3(b). Also in this case the intensity is distributed in narrow energy bands parallel to the *x*- and *y*-axis. While the spectra for $h\nu = 301$ eV and 313 eV could be obtained for the same spectrometer setting this was not possible for $h\nu = 324$ eV, because the photoelectron is outside the energy window. In order to capture the energies of interest the mean energy of both spectrometer was shifted by 7 eV towards higher values. Again we observe that the intensity is confined to narrow energy regions parallel to the *x*- and *y*-axis.

In a next step we compute sum energy spectra. We firstly performed separate analysis for coincidences associated to the decay of $2p_{1/2}$ and $2p_{3/2}$ photoelectron. In all the considered cases we found out that the E_{sum} spectra associated to the two different transitions (L_2VV and L_3VV) display identical line shapes. Thus, we will present in the following a comprehensive analysis with spectra associated to the whole corresponding 2D-energy distributions. The comparison of E_{sum} spectra obtained for different photon energies is facilitated by plotting the intensity as a function of $E_{sum}^{max} - E_{sum}$. Emission of pairs which involve states at the Fermi level occur at $E_{sum}^{max} - E_{sum} = 0$. This procedure is the equivalent of setting the binding energy zero at E_F in photoemission. This finally leads to the spectra presented in Fig. 4. For easier comparison of the line shape we have scaled the spectra so that the maximum intensity is unity. For all three spectra the onset of pair emission occurs for $E_{sum}^{max} - E_{sum} \approx 0$ eV, the spectra also resemble a triangular shape except for the high binding energy where it starts to level out at around $E_{sum}^{max} - E_{sum} \approx 15$ eV. Up to this point the spectra are essentially identical, only the tailing beyond $E_{sum}^{max} - E_{sum} \approx 15$ eV is different. This is however not an intrinsic effect, but a consequence of the energetic position of the spectral features with respect to the selected energy window of the spectrometer. For this we recall Fig. 3 and focus on the position of the blue diagonal line. In each of the three 2D-energy distributions this line marks

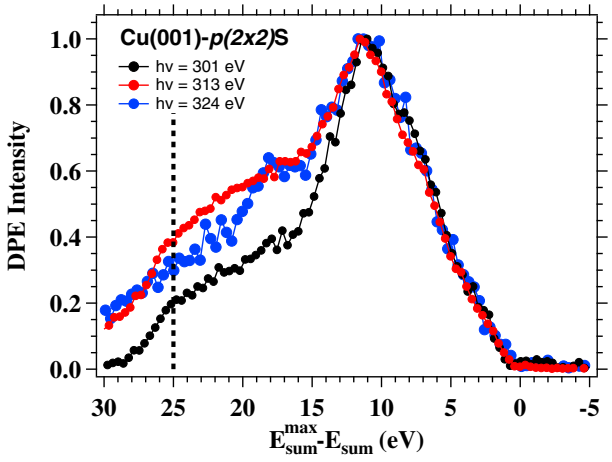

Fig. 4. Sum energy spectra obtained from the experiments with $h\nu = 301$, 313 and 324 eV. The dashed vertical line is the energy position of the blue diagonal line of Fig. 3 which is at $E^{max}_{sum} - 25$ eV. For better comparison we normalized the spectra such that the maximum intensity is unity. (For interpretation of the references to color in this figure legend, the reader is referred to the web version of this article.)

$E^{max}_{sum} - E_{sum} = 25$ eV. For $h\nu = 301$ eV this line is close to the left bottom corner, hence the length of the line is short. If we compare this with $h\nu = 313$ eV, we find the line further away from the bottom left hand corner and longer. The net effect is that the intensity levels at $E^{max}_{sum} - E_{sum} = 25$ eV are higher for $h\nu = 313$ eV in comparison to $h\nu = 301$ eV. This explains that the different intensities at the low binding energy tail are due to the limited energy range of the spectrometers. In all the 2D-energy spectra of Fig. 3 the whole Auger electron distribution is recorded by the spectrometers. Thus, the excess emission observed in the curves obtained at $h\nu = 313$ eV (red) and $h\nu = 324$ eV (blue) can be associated to electron pairs in which the S 2p photoelectron has been inelastically scattered.

Another important aspect of plotting E_{sum} spectra lies is the fact that the intensity peak at (135 eV, 135 eV) in Fig. 3(a) does not show up. This demonstrates that the feature observed in the 2D-energy spectrum is due to the overlapping of the vertical and horizontal intensity lines.

In the last part we prepared additional S overlayer structures. Growing first a Ni film onto the Cu(001) substrate and then commencing with the H_2S exposure leads to a c(2 × 2) structure of the overlayer. Sulfur overlayers on metal surfaces have been extensively studied in the past. There is consensus that for S/Cu(001) and S/Ni(001) the S atom is adsorbed at the hollow site [56–59]. The vertical distance of the S-layer to the underlying metal layer is for both systems in the range 1.29–1.32 Å. This means that in these two structures the S atom possesses a four-fold coordination where the bond length is 2.26 and 2.34 Å, respectively.

Experimental results on a S/O/Cu(001) sample suggest a structure in which half of the S atoms are incorporated within the first Cu layer [55]. These S atoms have 8 nearest neighbors compared to the S atoms on top which are 4 fold coordinated.

In Fig. 5 we compare the 2D-energy spectra obtained for the three S structures, the photon energy was 301 eV. The total true counts for the three spectra are 1.05×10^5, 4.16×10^4 and 3.13×10^4. It is apparent that these images display essentially the same features. The intensity is confined into rectangular regions parallel to the x- or y-axis. The solid diagonal line included in these distributions marks the energetic position of E^{max}_{sum}. Clearly, there is no discernible contribution of direct DPE from valence states. The spin-orbit splitting of the 2p-line is clearly visible for the S/Ni(001) structure although less sharp than for S/Cu(001). For the S/O/Cu(001) surface one can not identify the individual

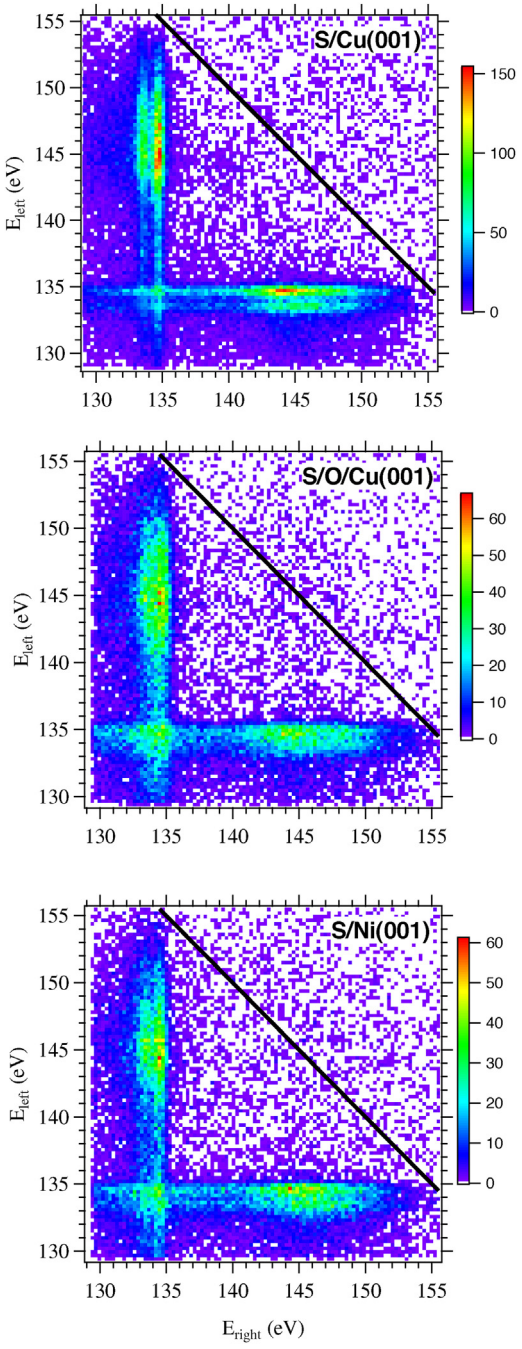

Fig. 5. 2D-energy spectra of different samples taken with $h\nu = 301$ eV photons, (a) S/Cu(001), (b) S/O/Cu(001) and (c) S/Ni/Cu(001). The solid diagonal line marks the energy position of E^{max}_{sum}.

contribution of the $2p_{1/2}$ and $2p_{3/2}$. We ascribe this to the two non-equivalent sites the sulfur atoms occupy in the S/O/Cu(001).

The next step consists in computing the E_{sum} spectra which are presented in Fig. 7(a) with the actual energy scale being $E^{max}_{sum} - E_{sum}$. In order to compare the spectra we normalized the intensity to unity for the maximum. In a recent paper we made use of first principle calculations to work out the surface density of states (DOS) of Cu(001)-p(2 × 2)S and we ascribed the main feature of the APECS spectrum to the possible two-hole final states. We pointed out that the main features in the Auger distribution arise from final states in which two vacancies are left in the bonding and non-bonding sulfur surface states [68]. We make use of the same methodology (see [68] for details) and extend the study to the other systems

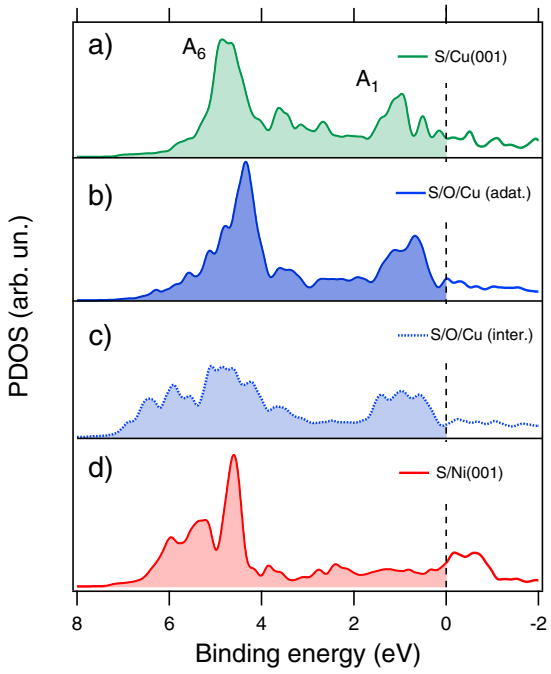

Fig. 6. DFT single-particle density of states projected onto the 3*p* orbitals of the sulfur atom for (a) S/Cu(001), (b) and (c) S/O/Cu(001) and (d) S/Ni(001). The DOS for S/O/Cu(001) has been calculated separately for adatoms (b) and interstitial atoms (c). The dashed line marks the energy position of the Fermi level.

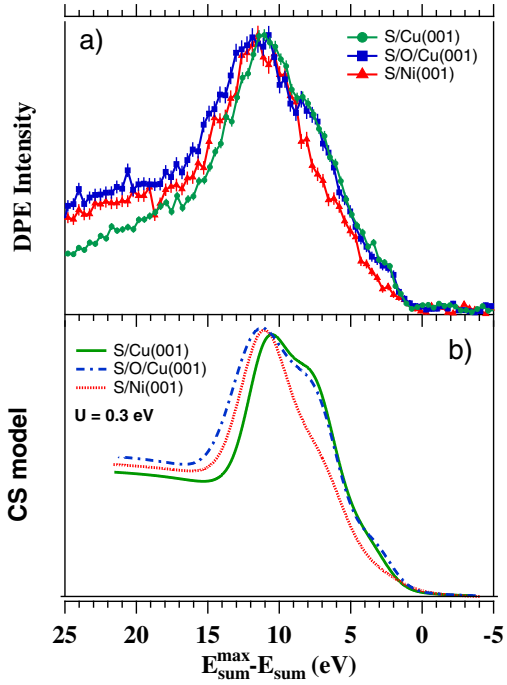

Fig. 7. (a) E_{sum} spectra computed from the 2D-energy distribution presented in Fig. 5. The photon energy was 301 eV. For better comparison we normalized the spectra such that the maximum intensity is unity. (b) Cini-Sawatzky (CS) model, for $U = 0.3$ eV, applied to the DOS of the three considered systems. S/Cu(001) (green continuous line), S/Ni(001) (dashed red line) and S/O/Cu(001) (dashed-dotted blue line). (For interpretation of the references to color in this figure legend, the reader is referred to the web version of this article.)

to explain the main differences among their sum energy spectra. Our first principles calculations were performed within the density functional theory framework. We used the SIESTA package which employs localized numerical atomic orbitals as basis set to solve the single-particle Kohn-Sham equations with periodic boundary conditions [69]. For the exchange and correlation potential we used the Perdew-Burke-Ernzerhof parametrization of the generalized gradient approximation (GGA) [70]. The interaction between ionic cores and valence electrons was described by norm-conserving Troullier-Martins pseudopotentials [71]. We used double-ζ polarized (DZP) basis sets for S and O while for Cu and Ni we enlarged the radii of the basis sets following the prescription described in [72]. An energy cutoff of 350 Ry has been sufficient for the real-space mesh. The first Brillouin zone was sampled with a grid equivalent to a $10 \times 10 \times 1$ Monkhorst-Pack grid [73] for the 1×1 surface unit cell. The systems were modeled by assuming a hollow absorption site for the S/Cu(001) and S/Ni(001) systems, while for S/O/Cu(001) we followed the model suggested in [55]. A seven layers thick slab with a lattice constant fixed to the theoretical equilibrium value has been considered. The geometric optimization of the two topmost surface layers together with the adsorbates was realized using the conjugated-gradient method until the residual forces were smaller than 0.01 eV/Å. Fig. 6 shows the calculated single-particle DOS for the three different systems we considered. The vertical scale is the same for all the plots. The S/Ni/Cu(001) interface has been modeled by S/Ni(001) because a 10 ML thick Ni film essentially decouples the electronic properties from the Cu substrate. The DOS of Cu is characterized by a region of large values in the binding energy range 1.5–5 eV, which is due to the 3*d* states occupied by 10 electrons. A *sp* band in the range E_F and 9 eV below is occupied by a single electron, which causes an almost constant DOS but at lower values than for the 3*d* states. The adsorption of S in a $p(2 \times 2)$ structure on Cu(001), Fig. 6(a), leads to the formation of antibonding (A_1) and bonding (A_6) state above and below the 3*d* DOS of the bare Cu(001) surface. A similar structure is observed for the adatoms on the O/Cu(001) surface (panel b). On the contrary for the interstitial atoms (panel c) we observe a weight transfer from the bonding level around 5 eV to more bound states at ~6 eV. A similar effect is observed when S atoms are adsorbed on Ni(001) in a $c(2 \times 2)$ configuration (panel d). Note that in this case the spin-summed DOS is reported. The main difference driven by the substrate variation lies in the fact that the antibonding state is pushed above the Fermi level. In a simplified picture this effect originates from a charge transfer from S to Ni where the S 3*p* electrons are hosted in the empty Ni 3*d* levels.

The line shape of the E_{sum} spectrum contains the effects of the correlation of the two holes left in the valence band which is directly linked to the correlation between the two emitted electrons. The simplest approach to describe the line shape is to use a self convolution of the DOS which neglects the electron–electron correlation [74]. However, a more detailed description of the two-particle line shape must take into account electronic correlations. This can be done by applying the Cini-Sawatzky (CS) model to the single-particle DOS [63,64]. Using the CS model we have recently determined a hole–hole correlation energy $U = 0.3 \pm 0.1$ eV for Cu(001)-$p(2 \times 2)$S surface states [68]. We used this value for the three investigated systems. A Shirley-type background was added to the calculations to account for inelastic losses of the electron pairs. The calculated curves were convoluted with a Gaussian profile of 1.1 eV full width at half maximum to account for the energy resolution of our setup. The computed spectra are shown in Fig. 7(b). The comparison between measured and calculated line shapes shows a very good agreement and the differences among the three experimental spectra are fully reproduced. It is then clear that a variation of the local environment around the sulfur adatoms hardly affects the strength of electronic correlations in the surface states.

The sum energy spectra of the two different sulfur reconstructions on copper show the same line shape for two-particle binding energies below 10 eV. Differences are observed in the high

binding energy side where the S/O/Cu(001) reconstruction (blue points) shows excess intensity with respect to S/Cu(001) (green points). In this reconstruction six S atoms are adsorbed on top of the surface and six are incorporated in the Cu matrix. The DOS projected on the S adatoms, Fig. 6(b), closely resembles the one for the p(2 × 2) reconstruction with the A_1 and A_6 levels slightly shifted to lower binding energy. The interstitial atoms, Fig. 6 c), show instead a reduction of the A_1 and A_6 intensity and the appearance of other states centered around 6 eV. Since the Auger decay is mainly localized on the atom of the initial ionization it makes sense to calculate the two particle line shape separately for adatoms and interstitial atoms. The total spectrum is then given by the sum of these two contributions as illustrated by the dashed-dotted blue line in Fig. 7(b). The differences observed in the high energy side of the sum energy spectra are essentially related to these interstitial sites that are responsible for the appearance of an extra feature at ∼12 eV and consequently for the broadening of the main two particle peak.

On the contrary the S/Ni(001) (red) curve presents an intensity reduction in the low two-particle binding energy side ($E_{sum}^{max} - E_{sum} \leq 8$ eV). This is due to a reduced density of states around the Fermi energy for this system. According to energy conservation (Eq. (1)), this portion of the spectrum is indeed ascribable to final states in which at least one of the two vacancies is close to E_F. This is a striking evidence of how the presence of an adsorbate species may totally change the surface electronic structure of a system. For the bare nickel surface we know that a high DOS is expected near E_F due to the partially filled 3*d* bands [75]. This is very different for copper where the 3*d* bands start 2 eV below the Fermi level. The adsorption of sulfur atoms and the formation of an hybrid valence band totally reverses the above scenario.

In the past years several ultraviolet photoemission (UPS) and ion neutralization spectroscopy (INS) experiments have been performed on Ni(001)-c(2 × 2)S. In all of these studies the bonding states were clearly observed [75–80]. Some of them showed an extra peak 2 eV below the Fermi level. The origin of this peak was unclear. Some authors associated it to a non-bonding S level [75,79] while some other considered it to contain emission from Ni *d*-band [77,78]. According to our experimental evidence it is now clear that no S state is expected within that binding energy region.

4. Conclusions

We performed electron–electron coincidence experiments of various sulfur-overlayers on metal surfaces. The focus was on the Auger decay following the excitation of the S 2*p* level. We find that the energy distributions follow the predictions of a two-step approximation of the decay. In this case the Auger electron line shape is identical to the line shape of the sum energy (E_{sum}) spectra. We observed that the line shape does not depend on the photon energy. Comparing three different sulfur-overlayer structures revealed that variation of the coordination or chemical nature of the S nearest neighbors leads to small but appreciable differences in the E_{sum} spectra. These can be understood in terms of electronic structure variations at the different interfaces. We observed a clear change in the density of states around the Fermi energy when we moved from a copper to a nickel substrate. In particular the sulfur induced anti-bonding state, completely filled for S/Cu, is empty for S/Ni. This is observed as a reduced intensity in the low two-particle binding energy region of the S/Ni coincidence spectrum.

The effects of larger sulfur coverage are observed in the high binding energy side of the surface valence band. These correspond to the appearance of additional bonding states around 6 eV binding energy and to the consequent broadening of the two-particle spectra.

It is worth noticing that a change of the environment around the sulfur atom does not lead to an appreciable variation of the strength of electron–electron interaction in the surface states.

Acknowledgements

We thank the BESSY II staff of the HZB, particularly W. Mahler and B. Zada, for excellent experimental conditions at the beamline. This work was partly supported by DFG via SFB 762.

References

[1] T.A. Carlson, Double electron ejection resulting from photo-ionization in the outermost shell of He, Ne, and Ar, and its relationship to electron correlation, Phys. Rev. 156 (1) (1967) 142, http://dx.doi.org/10.1103/PhysRev.156.142.
[2] C. Gazier, J. Prescott, Pairs of photoemitted electrons from potassium, Phys. Lett. A 32 (6) (1970) 425, http://dx.doi.org/10.1016/0375-9601(70)90036-8.
[3] P. Lablanquie, J.H.D. Eland, I. Nenner, P. Morin, J. Delwiche, M.J. Hubin-Franskin, Threshold behavior in single-photon double ionization of Argon, Phys. Rev. Lett. 58 (1987) 992, http://dx.doi.org/10.1103/PhysRevLett.58.992.
[4] H.W. Haak, G.A. Sawatzky, T.D. Thomas, Auger-photoelectron coincidence measurements in copper, Phys. Rev. Lett. 41 (26) (1978) 1825, http://dx.doi.org/10.1103/PhysRevLett.41.1825.
[5] R. Herrmann, S. Samarin, H. Schwabe, J. Kirschner, Two electron photoemission in solids, Phys. Rev. Lett. 81 (1998) 2148, http://dx.doi.org/10.1103/PhysRevLett.81.2148.
[6] F.O. Schumann, C. Winkler, G. Kerherve, J. Kirschner, Mapping the electron correlation in two-electron photoemission, Phys. Rev. B 73 (2006) 041404 (R), http://dx.doi.org/10.1103/PhysRevB.73.041404.
[7] P. Lablanquie, F. Penent, J. Palaudoux, L. Andric, P. Selles, S. Carniato, K. Buccaronar, M. Zcaronitnik, M. Huttula, J.H.D. Eland, E. Shigemasa, K. Soejima, Y. Hikosaka, I.H. Suzuki, M. Nakano, K. Ito, Properties of hollow molecules probed by single-photon double ionization, Phys. Rev. Lett. 106 (6) (2011) 063003, http://dx.doi.org/10.1103/PhysRevLett.106.063003.
[8] J. Berakdar, Emission of correlated electron pairs following single-photon absorption by solids and surfaces, Phys. Rev. B 58 (1998) 9808, http://dx.doi.org/10.1103/PhysRevB.58.9808.
[9] J.S. Briggs, V. Schmidt, Differential cross sections for photo-double-ionization of the helium atom, J. Phys. B: At. Mol. Opt. Phys. 33 (1) (2000) R1.
[10] T. Arion, U. Hergenhahn, Coincidence spectroscopy: past, present and perspectives, J. Electron. Spectrosc. Relat. Phen. 200 (2015) 222, http://dx.doi.org/10.1016/j.elspec.2015.06.004.
[11] T.J. Reddish, J.P. Wightman, M.A. MacDonald, S. Cvejanović, Triple differential cross section measurements for double photoionization of D_2, Phys. Rev. Lett. 79 (1997) 2438, http://dx.doi.org/10.1103/PhysRevLett.79.2438.
[12] L. Avaldi, A. Huetz, Photodouble ionization and the dynamics of electron pairs in the continuum, J. Phys. B: At. Mol. Opt. Phys. 38 (9) (2005) S861.
[13] J. Ullrich, R. Moshammer, A. Dorn, R. Dörner, L.P.H. Schmidt, H. Schmidt-Böcking, Recoil-ion and electron momentum spectroscopy: reaction-microscopes, Rep. Prog. Phys. 66 (9) (2003) 1463.
[14] J. Berakdar, J. Kirscher (Eds.), Correlation Spectroscopy of Surfaces, Thin Films, and Nanostrucutures, Wiley, Weinheim, 2004, http://dx.doi.org/10.1002/3527603425.
[15] J. Viefhaus, G. Snell, R. Hentges, M. Wiedenhöt, F. Heiser, O. Geßner, U. Becker, Interference effects between Auger and photoelectron studied by subnatural linewidth Auger-photoelectron coincidence spectroscopy, Phys. Rev. Lett. 80 (8) (1998) 1618, http://dx.doi.org/10.1103/PhysRevLett.80.1618.
[16] S.J. Schaphorst, A. Jean, O. Schwarzkopf, P. Lablanquie, L. Andric, A. Huetz, J. Mazeau, V. Schmidt, Interference effects in angular patterns of resonant double photoionization in neon, J. Phys. B: At. Mol. Opt. Phys. 29 (10) (1996) 1901.
[17] P. Bolognesi, M. Coreno, L. Avaldi, L. Storchi, F. Tarantelli, Site-selected Auger electron spectroscopy of N_2O, J. Chem. Phys. 125 (5) (2006), http://dx.doi.org/10.1063/1.2213254.
[18] V. Ulrich, S. Barth, S. Joshi, T. Lischke, A.M. Bradshaw, U. Hergenhahn, Separating the vibrationally resolved Auger decay channels for a CO core hole state, Phys. Rev. Lett. 100 (2008) 143003, http://dx.doi.org/10.1103/PhysRevLett.100.143003.
[19] F.O. Schumann, J. Kirschner, J. Berakdar, Mapping out electron–electron interactions at surfaces, Phys. Rev. Lett. 95 (2005) 117601, http://dx.doi.org/10.1103/PhysRevLett.95.117601.
[20] N. Fominykh, J. Berakdar, J. Henk, P. Bruno, Spectroscopy of the electron–electron interaction in solids, Phys. Rev. Lett. 89 (2002) 086402, http://dx.doi.org/10.1103/PhysRevLett.89.086402.
[21] F.O. Schumann, C. Winkler, J. Kirschner, Sensing the electron–electron correlation in solids via double photoemission, Phys. Status Solidi B 246 (2009) 1483, http://dx.doi.org/10.1002/pssb.200945203.
[22] J. Berakdar, H. Gollisch, R. Feder, Pair correlation in two-electron emission from surfaces, Solid State Commun. 112 (10) (1999) 587, http://dx.doi.org/10.1016/S0038-1098(99)00365-8.

[23] F.O. Schumann, C. Winkler, J. Kirschner, Correlation effects in two electron photoemission, Phys. Rev. Lett. 98 (25) (2007) 257604, http://dx.doi.org/10.1103/PhysRevLett.98.257604.

[24] F.O. Schumann, C. Winkler, J. Kirschner, F. Giebels, H. Gollisch, R. Feder, Spin-resolved mapping of spin contribution to exchange-correlation holes, Phys. Rev. Lett. 104 (8) (2010) 087602, http://dx.doi.org/10.1103/PhysRevLett.104.087602.

[25] G.A. Sawatzky, Auger photoelectron coincidence spectroscopy, in: R.P. Messmer, C.L. Bryant (Eds.), Auger Electron Spectroscopy, Academic Press, San Diego, 1988.

[26] E. Jensen, R.A. Bartynski, S.L. Hulbert, E. Johnson, Auger photoelectron coincidence spectroscopy using synchrotron radiation, Rev. Sci. Instrum. 63 (1992) 3013, http://dx.doi.org/10.1063/1.1142602.

[27] S.M. Thurgate, Coincidence measurements in the electron spectroscopies: surface studies, Surf. Interface Anal. 20 (1993) 627, http://dx.doi.org/10.1002/sia.740200804.

[28] A. Liscio, R. Gotter, A. Ruocco, S. Iacobucci, A.G. Danese, R.A. Bartynski, G. Stefani, Experimental evidence for extreme surface sensitivity in Auger-photoelectron coincidence spectroscopy (APECS) from solids, J. Electron Spectrosc. Relat. Phenom. 137–140 (2004) 505, http://dx.doi.org/10.1016/j.elspec.2004.02.099.

[29] O. Gunnarsson, K. Schönhammer, Dynamical theory of Auger processes, Phys. Rev. B 22 (8) (1980) 3710, http://dx.doi.org/10.1103/PhysRevB.22.3710.

[30] G.A. van Riessen, Z. Wei, R.S. Dhaka, C. Winkler, F.O. Schumann, J. Kirschner, Direct and core-resonant double photoemission from Cu(001), J. Phys.: Condens. Matter 22 (9) (2010) 092201.

[31] Z. Wei, F.O. Schumann, C.H. Li, L. Behnke, G. Di Filippo, G. Stefani, J. Kirschner, Dynamic screening probed by core-resonant double photoemission from surfaces, Phys. Rev. Lett. 113 (26) (2014) 267603, http://dx.doi.org/10.1103/PhysRevLett.113.267603.

[32] H. Aksela, A. Ausmees, O.P. Sairanen, S.J. Osborne, A.N. de Brito, A. Kivimäki, J. Jauhiainen, S. Svensson, S. Aksela, First observation on the photon energy dependence of the partial Auger transition rates in both the $4d_{\frac{3}{2}}$ and $4d_{\frac{5}{2}}$ Auger decay of Xe, Phys. Rev. Lett. 73 (1994) 2031, http://dx.doi.org/10.1103/PhysRevLett.73.2031.

[33] R.A. Bartynski, E. Jensen, S.L. Hulbert, Novel electronic properties of solids revealed by Auger-photoelectron coincidence spectroscopy (APECS), Phys. Scr. T41 (1992) 168.

[34] R.A. Bartynski, S. Yang, S.L. Hulbert, C.C. Kao, M. Weinert, D.M. Zehner, Surface electronic structure and off-site Auger transitions on TaC(111) observed with Auger-photoelectron coincidence spectroscopy, Phys. Rev. Lett. 68 (1992) 2247, http://dx.doi.org/10.1103/PhysRevLett.68.2247.

[35] C.P. Lund, S.M. Thurgate, A.B. Wedding, Auger photoelectron coincidence spectroscopy studies: trends in the $L_{2,3}$-$M_{4,5}M_{4,5}$ line shapes across the 3d transition-metal series, Phys. Rev. B 55 (1997) 5455, http://dx.doi.org/10.1103/PhysRevB.55.5455.

[36] G. Stefani, R. Gotter, A. Ruocco, F. Offi, F.D. Pieve, S. Iacobucci, A. Morgante, A. Verdini, A. Liscio, H. Yao, R.A. Bartynski, Photoelectron-auger electron coincidence study for condensed matter, J. Electron Spectrosc. Relat. Phenom. 141 (2–3) (2004) 149, http://dx.doi.org/10.1016/j.elspec.2004.06.005.

[37] T. Kakiuchi, M. Tahara, S. Hashimoto, N. Fujita, M. Tanaka, K. Mase, S.-I. Nagaoka, Surface-site-selective study of valence electronic states of a clean Si(111)-7×7 surface using Si$L_{23}VV$ Auger electron and Si 2p photoelectron coincidence measurements, Phys. Rev. B 83 (2011) 035320, http://dx.doi.org/10.1103/PhysRevB.83.035320.

[38] R. Gotter, F. Offi, A. Ruocco, F. Da Pieve, R. Bartynski, M. Cini, G. Stefani, Evidence for the collapse of short-range magnetic order in CoO at the Neel temperature, Europhys. Lett. 94 (3) (2011) 37008.

[39] M. Cini, E. Perfetto, R. Gotter, F. Offi, A. Ruocco, G. Stefani, Insight on hole–hole interaction and magnetic order from dichroic Auger-photoelectron coincidence spectra, Phys. Rev. Lett. 107 (21) (2011) 217602, http://dx.doi.org/10.1103/PhysRevLett.107.217602.

[40] R. Gotter, M. Sbroscia, M. Caminale, S.R. Vaidya, E. Perfetto, R. Moroni, F. Bisio, S. Iacobucci, G. Di Filippo, F. Offi, A. Ruocco, G. Stefani, L. Mattera, M. Cini, Monitoring antiferromagnetism via angle-resolved Auger photoelectron coincidence spectroscopy: the case of NiO/Ag(001), Phys. Rev. B 88 (9) (2013) 094403, http://dx.doi.org/10.1103/PhysRevB.88.094403.

[41] R. Gotter, G. Fratesi, R.A. Bartynski, F. Da Pieve, F. Offi, A. Ruocco, S. Ugenti, M.I. Trioni, G.P. Brivio, G. Stefani, Spin-dependent on-site electron correlations and localization in itinerant ferromagnets, Phys. Rev. Lett. 109 (12) (2012) 126401, http://dx.doi.org/10.1103/PhysRevLett.109.126401.

[42] J. Oudar, Sulfur adsorption and poisoning of metallic catalysts, Catal. Rev. 22 (2) (1980) 171, http://dx.doi.org/10.1080/03602458008066533.

[43] C.H. Bartholomew, Mechanisms of catalyst deactivation, Appl. Catal. A 212 (1–2) (2001) 17, http://dx.doi.org/10.1016/S0926-860X(00)00843-7.

[44] F.O. Schumann, R.S. Dhaka, G.A. van Riessen, Z. Wei, J. Kirschner, Surface state and resonance effects in electron pair emission from Cu(111), Phys. Rev. B 84 (2011) 125106, http://dx.doi.org/10.1103/PhysRevB.84.125106.

[45] K.J.S. Sawhney, F. Senf, M. Scheer, F. Schäfers, J. Bahrdt, A. Gaupp, W. Gudat, A novel undulator-based PGM beamline for circularly polarised synchrotron radiation at BESSY II, Nucl. Instrum. Methods A 390 (3) (1997) 395, http://dx.doi.org/10.1016/S0168-9002(97)00402-6.

[46] M. Abu-Joudeh, B. Davies, P. Montano, Leed, Auger, and electron energy loss studies of Ni epitaxially grown on Cu(100), Surf. Sci. 171 (1986) 331, http://dx.doi.org/10.1016/0039-6028(86)91084-8.

[47] F. Huang, M. Kief, G. Mankey, R. Willis, Magnetism in the few-monolayers limit: a surface magneto-optic Kerr-effect study of the magnetic behavior of ultrathin films of Co, Ni, and Co-Ni alloys on Cu(100) and Cu(111), Phys. Rev. B 49 (1994) 3962, http://dx.doi.org/10.1103/PhysRevB.49.3962.

[48] J. Shen, J. Giergiel, J. Kirschner, Growth and morphology of Ni/Cu(100) ultrathin films: an in situ study using scanning tunneling microscopy, Phys. Rev. B 52 (1995) 8454, http://dx.doi.org/10.1103/PhysRevB.52.8454.

[49] W. Platow, U. Bovensiepen, P. Poulopoulos, M. Farle, K. Baberschke, L. Hammer, S. Walter, S. Müller, K. Heinz, Structure of ultrathin Ni/Cu(001) films as a function of film thickness, temperature and magnetic order, Phys. Rev. B 59 (1999) 12641, http://dx.doi.org/10.1103/PhysRevB.59.12641.

[50] H.C. Zeng, R.A. McFarlane, K.A.R. Mitchell, A LEED crystallographic investigation of some missing row models for the Cu(100)$(2\sqrt{2}\times\sqrt{2})$R45°-O surface structure, Surf. Sci. 208 (1–2) (1989) L7, http://dx.doi.org/10.1016/0167-2584(89)91021-9.

[51] F. Jensen, F. Besenbacher, E. Laegsgaard, I. Stensgaard, Dynamics of oxygen-induced reconstruction of Cu(100) studied by scanning tunneling microscopy, Phys. Rev. B 42 (1990) 9206, http://dx.doi.org/10.1103/PhysRevB.42.9206.

[52] I.K. Robinson, E. Vlieg, S. Ferrer, Oxygen-induced missing-row reconstruction of Cu(001) and Cu(001)-vicinal surfaces, Phys. Rev. B 42 (1990) 6954, http://dx.doi.org/10.1103/PhysRevB.42.6954.

[53] D.E. Kuhl, R.G. Tobin, On the design of capillary and effusive gas dosers for surface science, Rev. Sci. Instrum. 66 (4) (1995) 3016, http://dx.doi.org/10.1063/1.1145588.

[54] M.L. Colaianni, I. Chorkendorff, Scanning-tunneling-microscopy studies of the S-induced reconstruction of Cu(100), Phys. Rev. B 50 (12) (1994) 8798, http://dx.doi.org/10.1103/PhysRevB.50.8798.

[55] M.L. Colaianni, P. Syhler, I. Chorkendorff, H_2S interaction with Cu(100)-(2 $\sqrt{2}times\sqrt{2}$) $R45^\circ$-O: formation of a metastable $\|_{05}^{52}$ sulfur surface reconstruction, Phys. Rev. B 52 (3) (1995) 2076, http://dx.doi.org/10.1103/PhysRevB.52.2076.

[56] D.H. Rosenblatt, J.G. Tobin, M.G. Mason, R.F. Davis, S.D. Kevan, D.A. Shirley, C.H. Li, S.Y. Tong, Normal photoelectron diffraction of c(2×2)O(1s)-Ni(001) and c(2×2)S(2p)-Ni(001), with Fourier-transform analysis, Phys. Rev. B 23 (8) (1981) 3828, http://dx.doi.org/10.1103/PhysRevB.23.3828.

[57] A.E. Schach von Wittenau, Z. Hussain, L.Q. Wang, Z.Q. Huang, Z.G. Ji, D.A. Shirley, Reevaluation of the p(2×2)S/Cu(001) structure using angle-resolved photoemission extended fine-structure spectroscopy, Phys. Rev. B 45 (23) (1992) 13614, http://dx.doi.org/10.1103/PhysRevB.45.13614.

[58] H.C. Zeng, R.A. McFarlane, K.A.R. Mitchell, Investigation with low-energy electron diffraction of the adsorbate-induced metal relaxations in the Cu(100)-(2×2)-S surface structure, Phys. Rev. B 39 (11) (1989) 8000, http://dx.doi.org/10.1103/PhysRevB.39.8000.

[59] E. Vlieg, I.K. Robinson, R. McGrath, Structure determination of Cu(100)-p(2×2)-S using X-ray diffraction, Phys. Rev. B 41 (11) (1990) 7896, http://dx.doi.org/10.1103/PhysRevB.41.7896.

[60] J.N. Andersen, Adsorption of H_2S on Ni(100): kinetics and structure, Surf. Sci. 192 (2–3) (1987) 583, http://dx.doi.org/10.1016/S0039-6028(87)81149-4.

[61] J. Viefhaus, L. Avaldi, G. Snell, M. Wiedenhöft, R. Hentges, A. Rhüdel, F. Schäfers, D. Menke, U. Heinzmann, A. Engelns, J. Berakdar, H. Klar, U. Becker, Experimental evidence for circular dichroism in the double photoionization of helium, Phys. Rev. Lett. 77 (19) (1996) 3975, http://dx.doi.org/10.1103/PhysRevLett.77.3975.

[62] J.H.D. Eland, O. Vieuxmaire, T. Kinugawa, P. Lablanquie, R.I. Hall, F. Penent, Complete two-electron spectra in double photoionization: the rare gases Ar, Kr, and Xe, Phys. Rev. Lett. 90 (5) (2003) 053003, http://dx.doi.org/10.1103/PhysRevLett.90.053003.

[63] M. Cini, Two hole resonances in the XVV Auger spectra of solids, Solid State Commun. 24 (9) (1977) 681, http://dx.doi.org/10.1016/0038-1098(77)90390-8.

[64] G.A. Sawatzky, Quasiatomic Auger spectra in narrow-band metals, Phys. Rev. Lett. 39 (8) (1977) 504, http://dx.doi.org/10.1103/PhysRevLett.39.504.

[65] P.A. Bennett, J.C. Fuggle, F.U. Hillebrecht, A. Lenselink, G.A. Sawatzky, Electronic structure of Ni and Pd alloys. III. Correlation effects in the Auger spectra of Ni alloys, Phys. Rev. B 27 (1983) 2194, http://dx.doi.org/10.1103/PhysRevB.27.2194.

[66] Y. Ma, P. Rudolf, E.E. Chaban, C.T. Chen, G. Meigs, F. Sette, Multiple sulfur sites in the Cu(100)p(2×2)-S surface structure, Phys. Rev. B 41 (8) (1990) 5424, http://dx.doi.org/10.1103/PhysRevB.41.5424.

[67] J.J. Yeh, I. Lindau, Atomic subshell photoionization cross sections and asymmetry parameters: $1 \le Z \le 103$, At. Data Nucl. Data Tables 32 (1) (1985) 1, http://dx.doi.org/10.1016/0092-640X(85)90016-6.

[68] G. Di Filippo, M.I. Trioni, G. Fratesi, F.O. Schumann, Z. Wei, C.H. Li, L. Behnke, S. Patil, J. Kirschner, G. Stefani, The LVV Auger line shape of sulfur on copper studied by Auger photoelectron coincidence spectroscopy, J. Phys.: Condens. Matter 27 (8) (2015) 085003.

[69] J.M. Soler, E. Artacho, J.D. Gale, A. Garcí a, J. Junquera, P. Ordejón, D. Sánchez-Portal, The Siesta method for ab initio order-n materials simulation, J. Phys.: Condens. Matter 14 (2002) 2745.

[70] J.P. Perdew, K. Burke, M. Ernzerhof, Generalized gradient approximation made simple, Phys. Rev. Lett. 77 (1996) 3865, http://dx.doi.org/10.1103/PhysRevLett.77.3865.

[71] N. Troullier, J.L. Martins, Efficient pseudopotentials for plane-wave calculations, Phys. Rev. B 43 (1991) 1993, http://dx.doi.org/10.1103/PhysRevB.43.1993.

[72] E.J.G. Santos, D. Sánchez-Portal, A. Ayuela, Magnetism of substitutional Co impurities in graphene: realization of single π vacancies, Phys. Rev. B 81 (2010) 125433, http://dx.doi.org/10.1103/PhysRevB.81.125433.
[73] H.J. Monkhorst, J.D. Pack, Special points for Brillouin-zone integrations, Phys. Rev. B 13 (1976) 5188, http://dx.doi.org/10.1103/PhysRevB.13.5188.
[74] J.J. Lander, Auger peaks in the energy spectra of secondary electrons from various materials, Phys. Rev. 91 (6) (1953) 1382, http://dx.doi.org/10.1103/PhysRev.91.1382.
[75] G.B. Fisher, The bonding of chalcogen overlayers on Ni (100), Surf. Sci. 62 (1) (1977) 31, http://dx.doi.org/10.1016/0039-6028(77)90426-5.
[76] T.W. Capehart, T.N. Rhodin, Selenium and sulfur bonding on Ni(111); angular resolved photoemission, Surf. Sci. 83 (2) (1979) 367, http://dx.doi.org/10.1016/0039-6028(79)90050-5.
[77] H.D. Hagstrum, G.E. Becker, Orbital energy spectra of electrons in chemisorption bonds: O, S, Se on Ni(100), J. Chem. Phys. 54 (3) (1971) 1015, http://dx.doi.org/10.1063/1.1674933.
[78] H.D. Hagstrum, G.E. Becker, Energy spectra of electrons in surface orbitals, Proc. R. Soc. A 331 (1586) (1972) 395, http://dx.doi.org/10.1098/rspa.1972.0186.
[79] T.T.A. Nguyen, R.C. Cinti, Directional UV photoemission from clean and sulphur saturated (100), (110) and (111) nickel surfaces, Surf. Sci. 68 (1977) 566, http://dx.doi.org/10.1016/0039-6028(77)90248-5.
[80] E.W. Plummer, B. Tonner, N. Holzwarth, A. Liebsch, Electronic structure of ordered sulfur overlayers on Ni(001), Phys. Rev. B 21 (10) (1980) 4306, http://dx.doi.org/10.1103/PhysRevB.21.4306.